Brillouin spectroscopy of polarization fluctuations in a $Rb_{1-x}(NH_4)_xH_2PO_4$ glass

Eric Courtens, René Vacher,* and Yves Dagorn†
IBM Zurich Research Laboratory, CH-8803 Rüschlikon, Switzerland
(Received 23 December 1985)

Brillouin scattering spectra of modes coupling linearly to the polarization have been obtained on a single crystal of the mixed ferroelectric-antiferroelectric system $Rb_{1-x}(NH_4)_xH_2PO_4$ with $x=0.35$, a concentration where a structural glass forms at low temperatures. A phenomenological description of the dielectric susceptibility is used which accounts perfectly for all aspects of the unusual line shapes observed. Crucial parameters of that theory are found in agreement with values derived from other independent measurements, such as dielectric-constant ones, giving strong support to the phenomenological description. Evidence for the existence of a broad distribution of relaxation times and of a dynamic central peak below the onset of freezing is presented. Besides the piezoelectric coupling effects, couplings of higher order in the polarization are found to play an important role as well, in particular for longitudinal modes.

I. INTRODUCTION

There is considerable current interest in the statistical mechanics of systems with randomly competing interactions. These can freeze into "glasses" at low temperatures. Better understanding of the associated dynamics could clarify the entire subject of the glassy state.[1] Among structurally frustrated mixed crystals,[2] the new[3] solid solutions of rubidium-dihydrogen phosphate (RDP) and ammonium-dihydrogen phosphate (ADP) have rapidly attracted considerable attention.[4] In that system, the competition is between the ferroelectric (FE) transition of RDP and the antiferroelectric (AFE) one of ADP, both characterized by specific orderings of the acid protons. The AFE order is induced by a competing hydrogen bonding of the ammonium ions.[5] The random distribution of the NH_4's in $Rb_{1-x}(NH_4)_xH_2PO_4$ or RADP produces the frustration. For $0.22 \lesssim x \lesssim 0.74$, both the low-temperature FE and AFE transitions are suppressed and the crystals manifest glasslike properties on cooling.[2,6] One great interest in these particular solid solutions, besides the ease of growing high-quality homogeneous and stable single crystals,[6] derives from the fact that in KH_2PO_4 (KDP) and its isomorphs a broad variety of susceptibility measurements can be performed. In this manner, it has been possible to establish that freezing in RADP is characterized by a wide distribution of relaxation times with a long-time cutoff whose temperature dependence could be measured over about 17 orders of magnitude in time.[7]

In this paper, we report on the measurement and interpretation of Brillouin scattering spectra from acoustic phonons linearly coupled to the polarization. This provides rather direct information on the corresponding frequency-dependent susceptibility at the high frequency of the Brillouin shift. The measurements were performed on samples with $x=0.35$, a concentration where the dielectric susceptibility is still rather large but where no FE transition occurs. In pure KDP, the FE transition is associated with an elastic instability of type I,[8] and the corresponding soft mode, together with defect-related and field-induced central-peak (CP) phenomena, have been observed in considerable detail.[9–12] In the RADP glasses, it is interesting to see what remains of the acoustic soft mode and also to follow the Raman soft mode down to Brillouin frequencies. In this way, we were able to gain dynamical information in the ~ 1 to ~ 0.01-cm^{-1} range, and this on illuminated sample volumes which are rather small ($\sim 10^{-2}$ mm^3) compared to the volumes used for other macroscopic measurements. Since small volumes are likely to be more homogeneous in their composition,[6] the latter point will become particularly important for studies near boundary lines of the phase diagram, where properties are likely to be strongly concentration dependent.

The theoretical description of the spectral profiles is developed in Sec. II along lines already tested successfully on KDP,[12] but extended here to the more general susceptibility that applies to the glasses.[7] Predictions that are in some fundamental ways different from those for KDP are found. The experimental details and necessary ancilliary information are given in Sec. III. The results for the xy-shear mode, which is the soft mode in the case of KDP,[9] are given in Sec. IV. Remarkable agreement between theory and experiment is obtained, which can be cross checked with the dielectric information on the piezoelectric coupling constant presented in Sec. III, and which interpolates the dynamics observed with Raman spectroscopy and with dielectric-constant measurements. In Sec. V, results on the longitudinal acoustic mode propagating along the xy diagonal are presented. In addition to its piezoelectric coupling, that mode is strongly affected by electrostriction in a manner similar to recent observations on the longitudinal acoustic mode propagating along the x axis.[13] This scattering geometry also reveals best the presence of a dynamic CP which is a feature in which the RADP glasses differ fundamentally from KDP. Finally, in Sec. VI, the essential results are summarized and compared with our current understanding of this system.

II. DIELECTRIC RESPONSE AND COUPLED SPECTRA

Crystals of the KDP family are piezoelectric already in their paraelectric phase, and it is thus necessary to consider their dielectric and elastic responses simultaneously. Including terms up to electrostriction, the constitutive equations are

$$\chi_{ij}^{-1}P_j - h_{ikl}e_{kl} - 2R_{ijkl}P_j e_{kl} = E_i \ , \tag{1a}$$

$$-h_{ikl}P_i - R_{ijkl}P_i P_j + C_{klmn}e_{mn} = \sigma_{kl} \ . \tag{1b}$$

Here, **P** and **e** are polarization and strain, respectively, while **E** and σ are the corresponding forces. With the polarization as an independent variable, the bare elastic stiffness tensor **C**, as well as the coupling tensors **h** and **R**, are only weakly dependent on temperature T. The T dependence of the bare elastic stiffness originates from lattice anharmonicity, and its corresponding imaginary part leads to a phonon linewidth below the present experimental resolution and can safely be ignored. The actual phonon linewidth, in the scattering geometries to be investigated, results from the coupling to the imaginary part of the bare dielectric susceptibility tensor χ. The piezoelectric tensor **h** has, for the point group $\bar{4}2m$ (D_{2d}), only two distinct nonvanishing components $h_{14}=h_{25}$ and h_{36}, where the last pair of indices is contracted. The electrostrictive tensor **R** has the same number of distinct components as the piezo-optic tensor, i.e., seven, while χ has two distinct components and **C** six. The spectra will first be discussed neglecting the contribution of **R**, to which we shall return at the end of this section.

Considering only the nonzero diagonal terms and dropping indices for simplicity, the susceptibility χ is written in terms of a distribution $g(\tau,T)$ of Debye relaxations of characteristic time τ,[7,14]

$$\chi(\omega,T)=\chi_B+\chi_0(T)\int_0^\infty \frac{g(\tau,T)}{1-i\omega\tau}d\ln\tau \ . \tag{2}$$

The distribution is normalized over $d\ln\tau$; χ_B corresponds to the relatively small background lattice contribution, assumed constant in frequency ω and T, while $\chi_0(T)$ is the very-low-frequency limit of the "critical part" of the susceptibility which is the main part of the paraelectric response. In KDP, $g(\tau,T)$ is very well approximated by a δ function,[11] while in RADP glasses, the distribution is broad in $\ln\tau$.[7] As defined in (1), χ is the "clamped" dielectric susceptibility that can be measured when the sample is sufficiently large for **e** to be zero at the measurement frequency. Contrarily, if ω is small compared to the sample resonant frequencies, no stress can develop and (1b) for σ_6 and with $\mathbf{R}=\mathbf{0}$ gives $-h_{36}P_3+C_{66}e_6=0$. Introducing the resulting value of e_6 in (1a) particularized to E_3, one finds for the "free" dielectric susceptibility parallel to the c axis $\chi_{FR}(\omega,T)$,

$$\chi_{FR}^{-1}(\omega,T)=\chi^{-1}-h_{36}^2/C_{66} \ . \tag{3}$$

It is the distribution (2) of relaxations that leads to dispersion and loss in the low-frequency dielectric constant $\epsilon_{FR}(\omega,T)=\chi_{FR}+1$ that has been observed below 30 K in RADP.[15] As the temperature is increased, the distribution $g(\tau,T)$ moves towards shorter characteristic times τ. As a result, for a fixed measurement frequency, there exists a temperature above which (2) and (3) effectively reduce to the "fully relaxed" values

$$\chi(0,T)=\chi_B+\chi_0(T) \ , \tag{4a}$$

$$\chi_{FR}(0,T)=\chi(0,T)Q/(Q-1) \ , \tag{4b}$$

where a dimensionless inverse coupling constant has been defined by

$$Q\equiv C_{66}/\chi(0,T)h_{36}^2 \ . \tag{5a}$$

The same definition has been particularly useful for the description of the KDP Brillouin spectra.[11,12] As seen from (4b), $Q(T)$ can be determined from a measurement of fully relaxed free and clamped dielectric constants, ϵ_{FR} and $\epsilon_{CL}=\chi+1$, respectively, since

$$Q^{-1}=1-(\epsilon_{CL}-1)/(\epsilon_{FR}-1) \ . \tag{5b}$$

One also sees from (4b) that $Q>1$ in the paraelectric phase, and that $Q=1$ corresponds to a FE transition where χ_{FR} diverges.

Brillouin scattering gives access to polarization fluctuations $\delta\mathbf{P}$ and thus to $\chi(\omega,T)$ in (2) by the fluctuation-dissipation theorem. In this work, scattering at 90° has been observed in the following two configurations.

(i) $T_1[100]$: seen in the geometry

$$\frac{\mathbf{x}+\mathbf{z}}{\sqrt{2}}\left[\mathbf{y},\frac{\mathbf{x}+\mathbf{z}}{\sqrt{2}}\right]\frac{\mathbf{z}-\mathbf{x}}{\sqrt{2}} \ ,$$

as illustrated in Fig. 1(a), with which shear waves propagating along **x** and polarized along **y** are probed. It is in this geometry that the soft acoustic mode is seen in KDP[9] and that the strongest coupling to polarization fluctuations is achieved in RADP glasses. In this case, the scattering wave vector **q** is given by

$$q=(2\pi/\lambda)(\tfrac{3}{2}n_0^2+\tfrac{1}{2}n_e^2)^{1/2} \ ,$$

where λ is the laser wavelength and n_0 and n_e are the ordinary and extraordinary indices, respectively.

(ii) L[110]: with the geometry **x**(**y**,**x**)**y**, as shown in Fig. 1(b), where only longitudinal wave propagating along

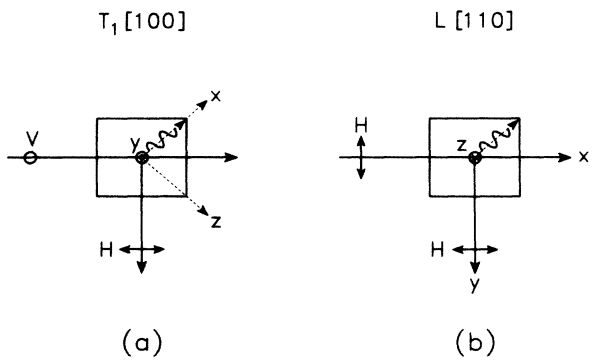

FIG. 1. Two scattering geometries used for the investigation. The laser and scattered-light polarizations are denoted by H or V and the wiggly lines show the phonon propagation directions.

$(\mathbf{x}-\mathbf{y})/\sqrt{2}$ and their coupling to fluctuations δP_3 are seen. This is the usual Raman scattering configuration to observe the B_2 mode in KDP.[16] For this polarization, the wave vector q is given by the above expression in which n_e is replaced by n_0.

In both cases, the relevant piezoelectric constant is h_{36}, while the elastic constant is C_{66} for $T_1[100]$ and $\frac{1}{2}(C_{11}+C_{12})+C_{66}$ for L[110]. Designating these constants by h and C, respectively, and ignoring $\mathbf{R}$, the equations of motion derived from (1) are, for either mode,

$$\chi^{-1}(\omega,T)\delta P - h\,\delta e = \delta E \ , \tag{6a}$$

$$-h\,\delta P + (C-\rho\omega^2/q^2)\delta e = \delta\sigma \ , \tag{6b}$$

where δP and δe are the fluctuating fields, δE and $\delta\sigma$ the corresponding fluctuating forces, and ρ the mass density. It is convenient to define the bare, or uncoupled, phonon frequency ω_a by

$$\omega_a \equiv q\sqrt{C/\rho} \ . \tag{7}$$

In the absence of FE or AFE transition, the weak decrease of $\omega_a(T)$ on heating can be described, in the Debye anharmonic approximation,[17] by

$$\omega_a(T)=\omega_a(0)-A\Theta F(\Theta/T) \ , \tag{8a}$$

where Θ is the Debye temperature and F the Debye function for the internal energy,

$$F(x)=\frac{3}{x^4}\int_0^x \frac{u^3}{e^u-1}du \ , \tag{8b}$$

as tabulated, for example, by Abramowitz and Stegun.[18]

The scattering strength depends on the piezo-optic constant p_{66} and on the electro-optic constant a_{36} that will be designated by p and a, respectively. Using the fluctuation-dissipation theorem, the scattered spectrum is, within a geometric factor,[12]

$$I(\omega,T)\propto\frac{kT}{\pi\omega}\mathrm{Im}\left[(a\ \ p)\begin{pmatrix}\chi^{-1} & -h\\ -h & \rho(\omega_a^2-\omega^2)/q^2\end{pmatrix}^{-1}\begin{pmatrix}a\\ p\end{pmatrix}\right] . \tag{9}$$

To evaluate this expression, it is convenient to use the following quantities:[12]

$$\Upsilon \equiv aC/ph \ , \tag{10a}$$

$$\kappa \equiv \kappa_R + i\kappa_I \equiv \int_0^\infty \frac{g(\tau,T)}{1-i\omega\tau}d\ln\tau \ . \tag{10b}$$

Υ determines the relative strengths of electro-optic and piezo-optic couplings, as can be seen by combining the constitutive equations (1), with the fluctuation in the inverse dielectric constant given by

$$\delta(\epsilon^{-1})_6 = a_{36}\,\delta P_3 + p_{66}\,\delta e_6 \ . \tag{11}$$

We also define, similar to (5a),

$$Q' \equiv C/(\chi_0+\chi_B)h^2 \ , \tag{12}$$

where $Q'=Q$ for $T_1[100]$, while $Q'=Q[\frac{1}{2}(C_{11}+C_{12})+C_{66}]/C_{66}$ for L[110]. With these definitions, (9) reduces to

$$I(\omega,T)\propto\frac{kT}{\pi\omega}\frac{\kappa_I p^2}{\chi_0 h^2}\times\frac{[1+\Upsilon(1-\omega^2/\omega_a^2)]^2}{\left[\kappa_R+\frac{\chi_B}{\chi_0}-Q'\left[1+\frac{\chi_B}{\chi_0}\right]\left[1-\frac{\omega^2}{\omega_a^2}\right]\right]^2+\kappa_I^2} \ . \tag{13}$$

Measurements performed over a very broad range of frequencies[7] suggest that in the glassy state of RADP the distribution $g(\tau,T)$ in (10b) can be derived from a distribution of barrier energies E, where the relaxation times are related to the barriers by the Vogel-Fulcher law[19]

$$\tau=\tau_0\exp[E/(T-T_0)] \ . \tag{14}$$

Brillouin measurements are not sensitive to the precise form of $f(E)$. For the present purpose, given that $f(E)$ is known to be rather flat in E,[7,15] the distribution is approximated by

$$f(E)=\begin{cases}0, & E<E_m \ , & \text{(15a)}\\ 1/(E_c-E_m), & E_m\le E\le E_c \ , & \text{(15b)}\\ 0, & E>E_c \ . & \text{(15c)}\end{cases}$$

Rather than $E_m=0$, recent dielectric scaling suggests that $E_m\simeq 60$ K.[20] This value affects only the normalization in (15b), while the corresponding minimum time $\tau_m=\tau_0[E_m/(T-T_0)]$ is, for $T>25$ K, anyway much shorter than the inverse of the Brillouin-phonon frequency, since $\nu_0=1/2\pi\tau_0$ is approximately 120 cm^{-1}.[7] The value of the high-energy cutoff time

$$\tau_c=\tau_0\exp[E_c/(T-T_0)]$$

falls within the range of the Brillouin time scales for $35\lesssim T\lesssim 70$ K, where it affects the shape of the spectra. With $g(\tau,T)d\ln\tau=f(E)dE$, using (10b), (14), and (15), one obtains straightforwardly,

$$\kappa_R = 1-\frac{1}{2}\frac{\ln[(1+\omega^2\tau_c^2)/(1+\omega^2\tau_m^2)]}{\ln\tau_c-\ln\tau_m} \ , \tag{16a}$$

$$\kappa_I = \frac{\arctan(\omega\tau_c)-\arctan(\omega\tau_m)}{\ln\tau_c-\ln\tau_m} \ . \tag{16b}$$

The general shape of the spectrum (13) is mainly governed by the poles of the denominator. The Brillouin peak is located approximately at ω_B given by

$$\kappa_R+\frac{\chi_B}{\chi_0}\cong Q'\left[1+\frac{\chi_B}{\chi_0}\right]\left[1-\frac{\omega_B^2}{\omega_a^2}\right] \ . \tag{17}$$

This phonon couples by Q' to the dielectric susceptibility. At high temperatures, where $\tau_c \ll 1/\omega_B$ (distribution I in Fig. 2), $\kappa_R\cong 1$ from (16a) and (17) reduces to

$$\omega_B\cong\omega_a\sqrt{(Q'-1)/Q'} \ . \tag{18}$$

In this case, the spectrum is nearly Lorentzian since $\kappa_I\propto\omega$. This is illustrated in Fig. 3 (curve I), which shows theoretical line profiles calculated from (13) using the

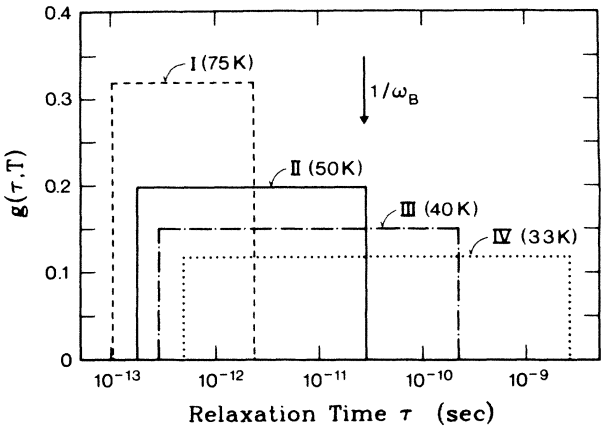

FIG. 2. Relaxation-time distributions at various temperatures. The values used for this figure are representative of those derived from the experiments. The inverse frequency of the $T_1[100]$ mode is indicated by the vertical arrow.

temperature-dependent parameters appropriate to the concentration $x=0.35$, as described below. Lorentzian fits to such spectra give ω_B, and using (18) together with the value of Q from the dielectric measurements allows the determination of the bare frequency ω_a. In the temperature region where ω_B approaches $1/\tau_c$, as illustrated by distribution II of Fig. 2, the maximum softening $\omega_a-\omega_B$ is observed. Indeed, above that temperature all relaxations are in equilibrium with the strain wave; the softening increases as T decreases because Q', proportional to the inverse susceptibility, decreases. Below that temperature, the slowest relaxations are not in equilibrium at ω_B, which causes $\kappa_R(\omega_B)$ to become smaller than 1 and thus ω_B to move towards higher frequencies as T is further decreased. Figure 3, curve II, illustrates a spectrum in the region of maximum coupling and two further spectra at lower temperatures (curves III and IV). The maximum width of the Brillouin peak does not occur in the region of maximum softening but at lower temperatures where the softening is of the order of one half its maximum, as illustrated by curve III in Fig. 3. This is similar to the situation in the case of the single relaxation time,[21] except that with a distribution the temperature region of the maximum width is rather broad.

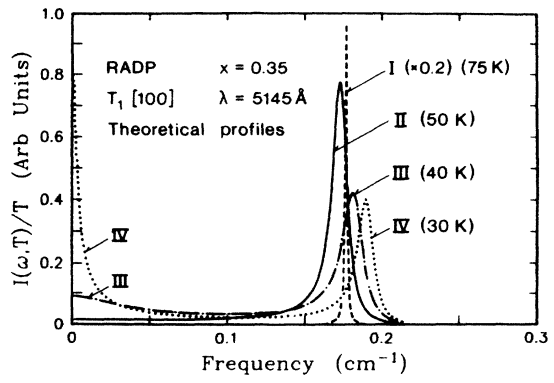

FIG. 3. Theoretical $T_1[100]$ spectra, before convolution with the instrumental function, corresponding to the distributions of Fig. 2. The parameters used for the calculation of the spectra are the experimental ones. The relative intensities, normalized by the absolute temperature, are significant.

At temperatures below the region of maximum coupling (curve III in Fig. 3) one also observes the growth of a dynamic central peak corresponding to the polarization fluctuations associated with the slow relaxations. The intensity of that CP emerges from the background intensity in the frequency region $\omega<\omega_B$. As the temperature is lowered further (curve IV in Fig. 3), the relaxation distribution extends rapidly to lower frequencies, the background decreases, and the CP becomes extremely narrow. This is rather different from the observations above the FE transition in pure KDP,[11] where the bare dielectric susceptibility always relaxes much faster than the shear mode observed in Brillouin scattering, so that a dynamic CP does not occur in the absence of a biasing field.[12,22] The simultaneous presence of a narrow dynamic CP and of a broadening of the acoustic phonon is the most prominent signature of the broad distribution of relaxation frequencies. To obtain such spectra, it is necessary to have relaxations, both near the Brillouin frequency, to broaden the phonon, and at much lower frequencies, to produce the quasi-elastic scattering.

In the numerator of (13), the factor containing Υ also affects the spectral shape. If $\Upsilon\ll 1$, the optical coupling occurs via the piezo-optic constant, and the above description is complete. However, if $\Upsilon\gg 1$, the coupling is purely electro-optic. In that case, the spectrum reflects pure polarization-polarization correlations which are effectively quenched at $\omega=\omega_a$ by the acoustic resonance at that frequency. This produces a zero in $I(\omega)$ at ω_a. For finite Υ, the effect is only an additional asymmetry of the line, with eventually a dip in the region of ω_a.

In the above discussion, the contributions of the electrostrictive tensor **R** of Eqs. (1) were neglected. Their effects can be quite dramatic, as revealed by recent Brillouin measurements of the L[100] phonon.[13] Including **R**, the equations of motion become nonlinear, and they cannot be written nearly as simply as (6) since they involve sums over the entire Brillouin zone. However, the phonon shift and damping can be estimated using Kubo's formalism.[23,24] The central result of such an analysis for RADP is that the polarization fluctuations $\delta\mathbf{P}$ must contain two components that are very distinct in their dynamics,[13]

$$\delta\mathbf{P}=\delta\mathbf{P}^s+\delta\mathbf{P}^d\ . \tag{19}$$

Here, $\delta\mathbf{P}^d$ is the usual dynamic part as considered in the above discussion of the spectral profile, while δP^s are much slower fluctuations (eventually static ones) that must already be present, with long-range correlations, at temperatures much above T_0. They correspond to an Edwards-Anderson-type order parameter[25] $\mathbf{q}^{\mathrm{EA}}$ that can be defined by

$$q^{\mathrm{EA}}_{mm}\equiv\frac{1}{V}\int_V[\delta P^s_m(\mathbf{r})]^2 d^3\mathbf{r}\ , \tag{20}$$

where the integration is over the volume V. The main contribution to the dispersion and attenuation of the L[100] phonon is found to arise from a Landau-Khalatnikov (LK) term[26] involving the product of the

dynamic correlations $\langle \delta \mathbf{P}^d \delta \mathbf{P}^d \rangle$ with the static ones $\mathbf{q}^{\mathrm{EA}}$. This gives a change in the elastic stiffness tensor $\mathbf{C}$ near $\mathbf{q}=0$,

$$\Delta C_{ijkl}^{\mathrm{LK}} \cong -4R_{mnij}R_{mnkl}q_{mm}^{\mathrm{EA}}\chi_{nn} , \tag{21}$$

where χ is the susceptibility defined in (2). In deriving that equation, it was assumed that the frequency dependence of $\chi(\mathbf{q},\omega)$ is rather constant throughout the Brillouin zone, so that χ can be replaced by its $\mathbf{q}=0$ value and can be factored outside the integral over the zone.

Similarly to (21), the elastic stiffness changes associated with piezoelectricity, using the Kubo formalism, can be written[24]

$$\Delta C_{ijkl} \cong -h_{nij}h_{nkl}\chi_{nn} . \tag{22}$$

Comparing (21) and (22), one sees that the electrostrictive Landau-Khalatnikov term has just the form of an additional piezoelectric contribution. Its main effect can roughly be accounted for by an increase of the effective piezoelectric constant, from h to h^{eff}, with

$$(h^{\mathrm{eff}})^2 = h^2 + 4R^2 q^{\mathrm{EA}} , \tag{23}$$

where $R^2 q^{\mathrm{EA}}$ is the appropriate mean of (21) for the scattering geometry of interest. Using the abbreviations $q_{ii}^{\mathrm{EA}} = q_i$ and $\chi_{ii} = \chi_i$, one finds, for $T_1[100]$, $R^2 q^{\mathrm{EA}} = 2R_{1212}^2 q_1$, while for L[110],

$$R^2 q^{\mathrm{EA}} = \tfrac{1}{2}(R_{1111}+R_{1122})^2 q_1 \chi_1/\chi_3 + R_{3311}^2 q_3 + 2R_{1212}^2 q_1 .$$

The values of the electrostrictive tensor components are not available to estimate those expressions. However, one can note that the tensor $\mathbf{R}$ gives the stress at zero strain. It is related to the tensor $\mathbf{Q}$ that gives strain at zero stress by $R_{ijkl} = Q_{ijmn}C_{mnkl}$. Except for the zeroes imposed by symmetry, there are no particular conditions on the relative sizes of the components of $\mathbf{Q}$. Since $C_{66} \ll C_{11}$, the component R_{1212} associated with pure shear is thus likely to be smaller than some of the other components of $\mathbf{R}$, such as R_{1111}. This is indeed borne out by experiment. As explained in Sec. IV, the $T_1[100]$ spectra can be accounted for quantitatively using the piezoelectric coupling alone. The resulting values of the coupling constant agree with those measured dielectrically. This is not the case for the L[110] spectra as shown in Sec. V. In that case, about one-half of the coupling observed is not of piezoelectric origin and it is thus assigned to electrostriction.

III. EXPERIMENTAL PROCEDURE AND AUXILIARY RESULTS

Brillouin scattering was excited with the 5145-Å line of an argon-ion laser operating on a single mode at ~200 mW. It was observed at 90° on the $T_1[100]$ and L[110] modes, as discussed in Sec. II. The scattered light was analyzed with a triple-pass Fabry-Perot interferometer with a plate spacing of 0.900 cm for the $T_1[100]$ and of 0.375 cm for the L[110] scattering geometries, respectively. The interferometer used is the first half of a tandem Sandercock system operating with its usual feedback electronics.[27] As the samples were of rather high clarity, additional elastic light required for the feedback control of the instrument was switched on and off near the middle of each scan using a high-speed shutter. The scans were performed over little more than three orders, and the outer two orders, not perturbed by the additional light, were kept for data evaluation. This also allows, at least in principle, the investigation of CP-type phenomena, provided the crystal quality is sufficiently high and any other source of stray light sufficiently low. The detection chain that follows the collection hole has been described elsewhere.[28] The photocounts were accumulated in 1024 channels of a multichannel analyzer from which they could be transferred to the main-frame computer.

For the analysis, the centers of the interferometer orders are determined and the counts are numerically redistributed among 300 virtual channels per order. These data are then fitted to the expected line shape obtained by the convolution of the instrumental profile with the theoretical spectrum of Eq. (13) folded over two interferometer orders. The instrumental profile is determined from 21 channels at the center of the spectrum and the latter is fitted over the outer 80% of the free-spectral range. This corresponds to a conservative estimate of the part of the free-spectral range that is practically unperturbed by elastic light. The fits are performed with Marquardt's nonlinear least-squares algorithm,[29] normalizing the deviations in each channel by the square root of the number of counts per channel.[11] In this way, the calculated mean-square deviation is the chi square appropriate to a Poisson statistic of photocount arrivals.

The samples used in these experiments were two rectangular blocks, 6 to 8 mm on the side, cut to an accuracy of better than 0.5° with the orientations shown in Fig. 1. They were derived from high-quality single crystals whose composition had been checked by an x-ray measurement of the lattice parameters.[6] The cryostat was either a CTI 21SC Cryodyne closed-cycle refrigerator for temperatures down to ~20 K, or a He gas-flow unit for lower temperatures. In the closed-cycle refrigerator, the samples were mounted in vacuum and enclosed in a sample holder in which they made contact with heat-conducting grease. The temperature was controlled to better than ±0.1 K and measured to ±0.01 K by a Si-diode thermometer placed on the sample holder. Each sample was carefully aligned in all directions using the reflections from the sample faces. To this effect, a reference beam propagating at 90° to the exciting laser beam was also used.

The refractive indices, needed for the evaluation of the momentum exchange q as explained in Sec. II, were measured using a 30° prism of RADP with its edge parallel to the c axis. The prism was placed in the closed-cycle refrigerator at approximately the minimum deviation angle for an incident 5145-Å laser beam. The temperature dependence of the angular deviation was measured with a 0.05 mrad relative accuracy for each polarization. The room-temperature indices were checked independently with a conventional goniometer. These results are summarized in Fig. 4.

The dielectric constant of a thin (001) plate provided with evaporated gold electrodes was measured with an automated bridge and temperature-control system. Data at

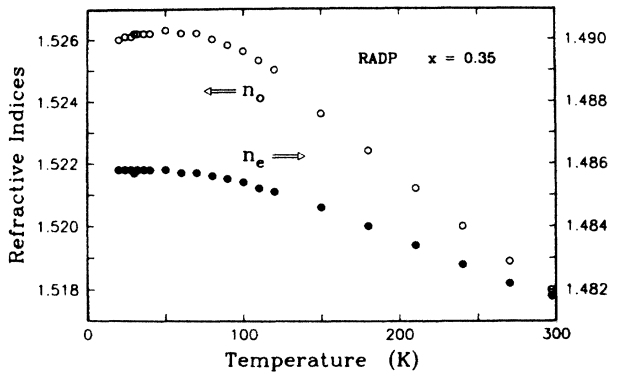

FIG. 4. Ordinary and extraordinary indices measured at $\lambda=5145$ Å.

four typical frequencies are shown in Fig. 5. The low-frequency curves illustrate the onset of dispersion below ~ 25 K. This dispersion is also associated with loss, not shown in Fig. 5.[15,20] Above ~ 25 K, all low-frequency curves coincide with the "fully relaxed" ϵ_{FR} $(\omega=0,T)$. Strong piezoelectric resonances occur in the region between 100 kHz and 1 MHz. Above these resonances, the sample is effectively clamped, as illustrated by the 10-MHz curve. Below ~ 35 K, the 10-MHz result is also affected by dispersion related to the distribution of relaxation times $g(\tau,T)$. Using ϵ_{FR} and ϵ_{CL} one calculates the coupling constant Q with (5b). The result is displayed in Fig. 6. At temperatures below the vertical arrow on that plot, the calculated Q decreases rapidly. This is due to dispersion in the 10-MHz measurement which invalidates those values of Q. In view of the very small difference between ϵ_{FR} and ϵ_{CL} in the region 150–300 K (Fig. 5), the use of the raw data for the calculation of Q at those temperatures leads to a considerable scatter. It is then better to fit both ϵ_{FR} and ϵ_{CL} to Curie-Weiss expressions, and to use the results of those fits for the calculation of Q. The fits are indistinguishable from the experimental curves on the scale of Fig. 5, and they lead to the smooth result shown on Fig. 6. The fits also give the value of the background dielectric constant $\epsilon_B=8$ which can then be used to calculate the small correction term χ_B/χ_0 in (13), with $\chi_B/\chi_0=(\epsilon_B-1)/(\epsilon_{CL}-\epsilon_B)$. The result is also displayed in Fig. 6, and it is valid down to the temperature indicated by the vertical arrow. For fits below that temperature, the ratio χ_B/χ_0 was assumed equal to its minimum value, a fair approximation in view of the small effect of that correction term.

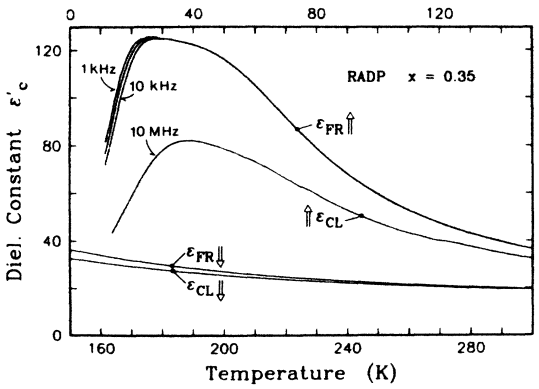

FIG. 5. Real part of the dielectric constant below the piezoelectric resonances (at 1, 3, and 10 kHz) and above them (at 10 MHz). The abcissa on top applies to the upper curves and the one below to the lower curves, as shown by the arrows.

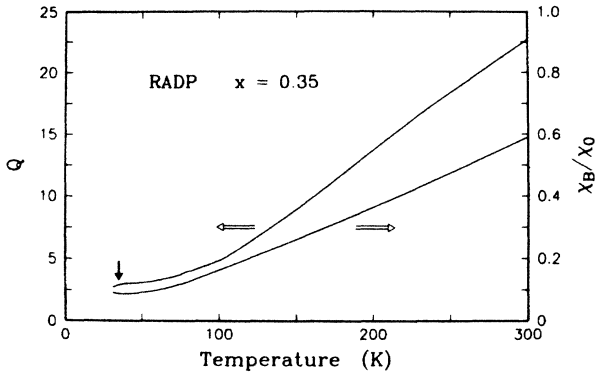

FIG. 6. Piezoelectric coupling parameter Q and the correction factor χ_B/χ_0 derived from the dielectric results of Fig. 5.

IV. T_1[100] SPECTRA

Typical T_1[100] spectra are presented in Fig. 7. With the elastic line centered on channel 0, the frequency range

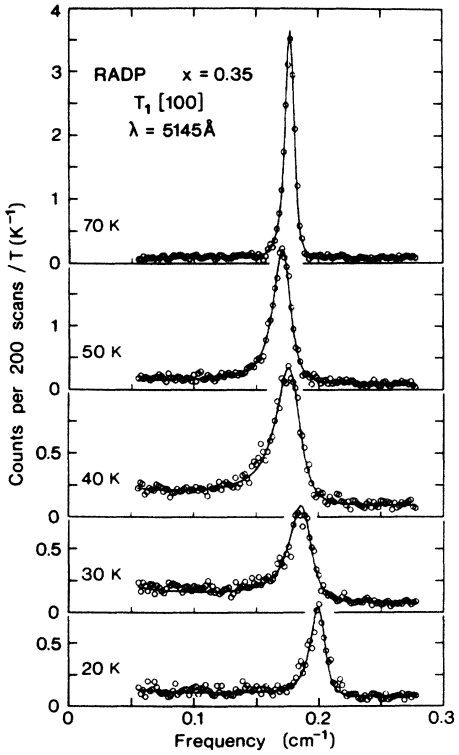

FIG. 7. Five typical T_1[100] spectra. The open circles are counts per virtual channel divided by the absolute temperature. The solid curves are fits with $\Upsilon=2$ and the other parameters, as explained in the text. The relative intensities are significant.

shown corresponds to channels 30 to 150. It is the one actually used for the fits. The elastic line is, in each case, considerably out of scale, with peaks ranging from 22 at 70 K to 205 at 20 K, on the ordinate scale of Fig. 7. The full width at half height of the elastic line is only ~ 4 channels, and its wing contributes to the channels used for the fits much less than the height of the statistical fluctuations, as will become clear later. The ordinates in Fig. 7 are normalized by the absolute temperature, for easier comparison of the relative integrated spectral intensities given by the sum rule:[12]

$$I \propto kT\frac{p^2}{C}[1+(1+\Upsilon)^2/(Q'-1)] . \quad (24)$$

The spectra of Fig. 7 are obviously all broadened beyond the width of the instrumental profile. The peak position reveals a maximum softening at ~ 50 K, while the maximum width of the Brillouin line occurs in the region between 40 and 30 K. The apparent decrease in intensity of the Brillouin line at the lowest temperatures, most obvious for the spectrum at 20 K, is to be related to a transfer of intensity into a dynamic CP that becomes masked by the elastic scattering, as will be discussed below.

The experimental profile predicted by Eq. (13), with κ given by (10b) and (16), depends on the following quantities: (i) the bare phonon frequency ω_a; (ii) the piezoelectric coupling coefficient Q'; (iii) the low-frequency cutoff $\nu_c = 1/2\pi\tau_c$ in the distribution of relaxation times, the high-frequency cutoff $\nu_m = 1/2\pi\tau_m$ being fixed at $\nu_0 \exp[E_m/(T-T_0)]$, with $\nu_0 = 120$ cm^{-1}, $E_m = 60$ K, and $T_0 = 8.7$ K;[7,20] (iv) the relative strength of the electro-optic and piezo-optic couplings given by the parameter Υ; (v) the spectral intensity; and (vi) a constant background that accounts for contributions from the dark counts of the photomultiplier and from the parasitic light. In principle, the measured spectra contain enough information to find the following six parameters: (i) the peak position of the phonon; (ii) its linewidth; (iii) the asymmetry of the base line from above ω_B to below ω_B, and the associated CP; (iv) an eventual dip near ω_a, related to Υ; (v) the spectral intensity; and (vi) the broad background intensity. However, as the inelastic CP is considerably masked by the elastic light, and in view of the finite spectral resolution, an independent determination of all six parameters can only be attempted in practice in the temperature range where the coupling strongly affects the phonon profile, which in this case is from 40 to 70 K. This is also the temperature range for which ν_c is expected to fall approximately within the frequency range of the measurement, i.e., from 0.05 to 0.3 cm^{-1}. At temperatures below 40 K, where $\omega_B/\nu_c \gg 1$, it can be seen from (13) and (16) that the position and shape of the phonon peak are essentially determined by the product $Q'\ln(\nu_m/\nu_c)$. An independent determination of Q' and ν_c is thus difficult at those temperatures. It could only be done reliably if the fully elastic CP were so weak that a good observation of the quasi-elastic CP shown in Fig. 3 would be possible. As this is not the case, we have fitted in that region with either ω_a, Q', or ν_c fixed, as explained below. Above 70 K, but below ~ 100 K, there remains very little width beyond that of the instrumental profile. Hence, the value of ν_c has a minor influence on the calculation of the spectrum. Indeed, from (16) one sees that $\kappa_R \cong 1$ and that $\kappa_I \cong 0$ at the Brillouin frequency at those temperatures. In that region, fits can be obtained fixing Q' to its value extracted from the dielectric data and extrapolating ν_c from low-temperature measurements. Above 100 K only the line position can be extracted. This has been done with Lorentzian fits, which are mostly excellent at those temperatures.

Figure 8 shows the phonon positions obtained from such Lorentzian fits over the entire temperature range (open circles). Although such fits are only fully satisfactory above 100 K, this gives an idea of the phonon softening. All 13 spectra measured in the range of strong coupling (40 to 70 K) were fitted with all six parameters free. The bare phonon frequencies obtained from these free fits are the open triangles, which are seen to be much above the open circles. The large difference between these frequencies is due to the piezoelectric coupling, as indicated in (17). Above 100 K, (18) applies. Since $Q = Q'$ in the present case, taking Q from the dielectric measurement (Fig. 6), one calculates from the coupled phonon frequencies (open circles) the corresponding bare frequencies ω_a shown by the closed circles. The latter can be fitted to a Debye internal energy curve, following Eq. (8). For that fit, we used the Debye temperature extracted from an x-ray measurement of the lattice volume, $\Theta = 384$ K.[30] The result of this fit is the solid curve in Fig. 8. It passes through the open triangles within their accuracy and properly connects to the open circles at the lowest measurement temperatures where the coupling vanishes. The closed triangles will be explained below.

Figures 9 and 10 depict other results from the free fits in the range 40 to 70 K. Figure 9 is a presentation of the values of Q' and Υ. The curve through the points Q' is the value of Q from the dielectric results. One notes the excellent agreement between the two independent determinations of the piezoelectric coupling. On the other hand, the values of Υ derived from the free fits do show a considerable scatter. The shape of the spectrum is rather insensitive to Υ. A better determination of this parameter would require static measurements of all quantities enter-

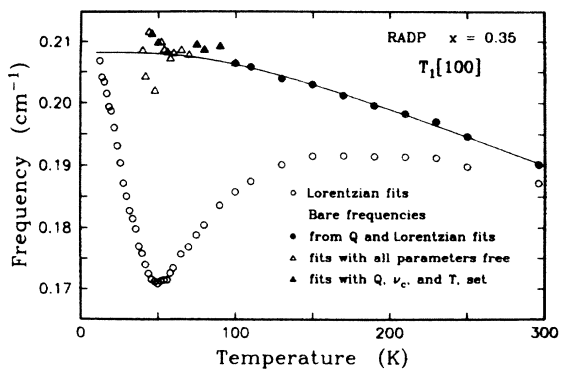

FIG. 8. Various determinations of the coupled and the bare phonon frequencies for the $T_1[100]$ mode. The coupled frequencies, obtained from simple Lorentzian fits, are shown by open circles.

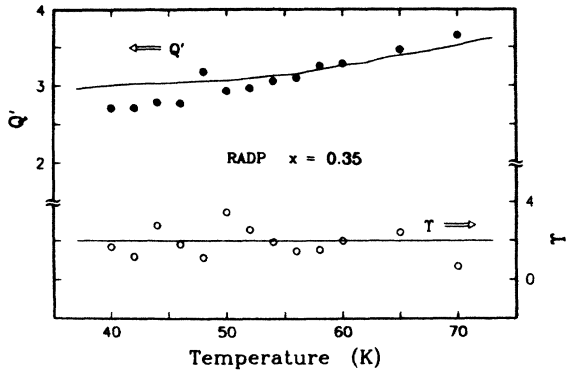

FIG. 9. Values of Q' and Υ obtained from fits with all parameters free in the strongly coupled region (40 to 70 K). The solid curve through the points for Q' is from the dielectric measurements (Fig. 6) with no adjustable parameter.

ing (10a), or a careful scattering-intensity measurement, as will be made clear shortly. For the present purpose, since the spectra have little sensitivity to Υ, and as the parameters in (10a) have only a weak temperature dependence, Υ can be approximated by its temperature-independent mean, $\Upsilon \cong 2$. This is demonstrated by the solid curves in Fig. 7, which are excellent fits obtained with Υ fixed to the value 2. Figure 10 is a semilogarithmic presentation of the cutoff frequency ν_c, where the abscissa is $(T-T_0)^{-1}$, with $T_0=8.7$ K, as suggested by the Vogel-Fulcher law (14). The open triangles are the values obtained from the free fits. The solid line is taken from an independent determination covering about 17 orders of magnitude in frequency.[7] It corresponds to $\nu_0=116$ cm^{-1} and $E_c=268$ K. One notes the excellent agreement between this line and the results of the free fits.

The spectra below 40 K have been fitted with ω_a fixed by the Debye curve of Fig. 8 and Q' fixed by its dielectric value extrapolated by a constant below 35 K. The results are consistent with the Vogel-Fulcher law at least down to $\nu_c \cong 10^{-5}$ cm^{-1} around 25 K. The solid lines in Fig. 7 for $T=30$ and 20 K were obtained by fixing ν_c to the value of the Vogel-Fulcher law, ω_a to the Debye value, and fitting only for Q. One observes that very good fits are obtained in that way, including the onset of a dynamic CP for the 30-K curve, to which we shall return shortly.

In the region $70 < T < 100$ K, very good fits are obtained with Q' fixed to the dielectric value, ν_c fixed by the Vogel-Fulcher law, and Υ set equal to 2. They yield the values of ω_a shown by the closed triangles in Fig. 8, which fall on the Debye curve within their accuracy.

We now return to the question of the integrated spectral intensities. Figure 11 displays the central section of the measured 30- and 20-K spectra of Fig. 7, on an extended abscissa scale. The vertical scale applies to the open circles. The closed circles show the instrumental function for the 30-K measurement, on a scale which has been contracted by a factor of $\simeq 73$. This peak is mostly due to elastic scattering. The closed triangles show the corresponding line for the 20-K spectrum, adjusted to the same peak intensity, emphasizing the good reproducibility of the instrumental profile. The scale of the 20-K spectrum (open triangles) is such that the two spectra with open symbols coincide at elastic peak ($\omega=0$). Since the quasi-elastic CP is expected to be extremely narrow at 20 K and broader at 30 K, the difference between these two spectra can give an indication of the presence of a quasi-elastic CP in the 30-K spectrum. An over-intensity is evident in the region $0.02 \leq \omega \leq 0.04$ cm^{-1} in the 30-K measurement. It indicates the presence of a quasi-elastic feature in the wing of the fully elastic CP. This quasi-elastic scattering accounts for the apparent loss of integrated intensity on lowering the temperature in Fig. 7. To further examine this point, the Brillouin spectral intensities, as shown in Fig. 7, extrapolated horizontally to $\omega=0$ in the

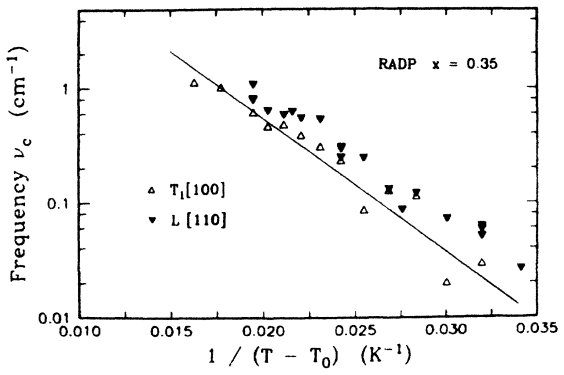

FIG. 10 Cutoff frequencies ν_c obtained from free fits to the $T_1[100]$ spectra (open triangles) and L[110] spectra (closed triangles). In the latter case, Q' was fixed to Q'' in (25b). The solid line is the Vogel-Fulcher fit derived from measurements covering about 17 orders of magnitude in frequency (Ref. 7). $T_0=8.7$ K is taken from that reference.

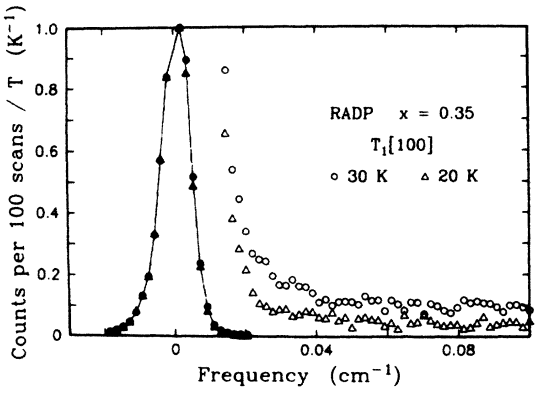

FIG. 11. Comparison of the low-frequency region of the $T_1[100]$ spectra at 30 and 20 K. The ordinate scale applies to the 30-K spectrum (open circles). The (mostly elastic) CP is illustrated for both the 30-K (closed circles, reduction factor $\simeq 73$) and the 20-K spectrum. The open triangles show the 20-K spectrum on a scale such that at $\omega=0$ its maximum coincides with that of the 30-K spectrum (open circles).

region $\omega < 0.055$ cm^{-1}, minus the broad background, have been integrated, divided by the absolute temperature, and normalized by the number of scans. The relative values of these intensities are expected to be meaningful within approximately $\pm 10\%$. The result is shown in Fig. 12. It is compared to the value of I/T from (24), calculated with $\Upsilon = 1.8$ (which is within the accuracy of our determination in Fig. 9) and with Q' equal to its dielectric value. The only free parameter is the scale constant between the points and the calculated curve. The agreement is truly remarkable down to ~ 40 K. At lower temperatures, the dielectric value of Q is not well known, owing to the relaxation in the 10-MHz dielectric-constant measurement. However, one expects that the solid curve should continue to rise moderately below 40 K, while the experimental phonon intensities are clearly seen to decrease. This is further evidence for the presence of a considerable quasielastic CP in the region below 0.055 cm^{-1}.

V. L[110] SPECTRA

In the L[110] geometry, the spectra, whose general aspect is similar to Fig. 7, differ from the $T_1[100]$ ones mainly by the larger value of the effective elastic constant C. This produces a larger bare phonon frequency (7), a larger relative importance of the electro-optic coupling given by Υ in (10a), and a larger inverse piezoelectric coupling constant Q' per (12). As a result, the phonon line is harder and narrower, the intensity dip at $\omega = \omega_a$ is more pronounced, and the dynamical CP is easier to observe. In addition, it will be seen that the electrostrictive terms are now of importance so that h in Eq. (12) will have to be replaced by a larger h^{eff}, as suggested by (23).

Figure 13 presents the coupled and the bare phonon frequencies obtained for the L[110] mode. The coupled phonon frequencies, derived from Lorentzian fits, should be compared to those of Fig. 8. It is immediately apparent that the frequency is about a factor of 3 higher for the L[110] mode and that the piezoelectric coupling is much

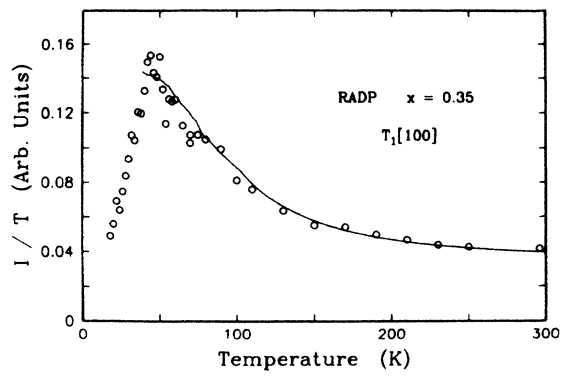

FIG. 12. Integrated intensity of the $T_1[100]$ phonon line, as explained in the text. The solid curve is derived from Eq. (24), with only the vertical scale as an adjustable parameter. The sharp decrease below ~ 40 K is interpreted as a loss of intensity into a dynamic CP, which is masked to a great extent by elastic defect scattering.

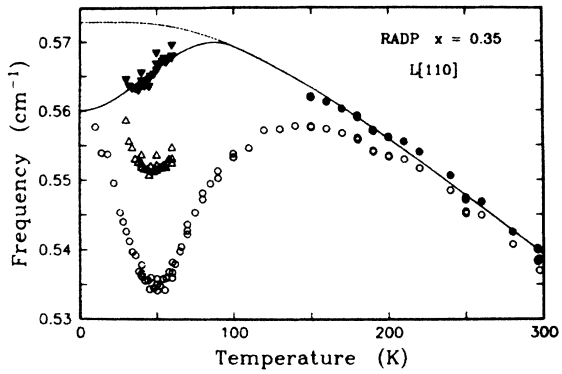

FIG. 13. Coupled (open circles) and bare frequencies derived from the L[110] spectra. The open triangles are values obtained ignoring the possibility of electrostrictive coupling. The closed triangles include the electrostrictive coupling. The closed circles are bare frequencies. The solid curve includes anharmonicity and the effect of an Edwards-Anderson order parameter. The dashed curve is a low-temperature extrapolation of the Debye function alone.

weaker since the softening in the region of 50 K is only about 5% of the bare frequency, as opposed to about 20% in Fig. 8. As the phonons are less coupled, it is also more difficult to extract values for all six parameters in completely free fits. In a first fitting attempt, one can try to analyze the spectra obtained between 30 and 60 K, fixing

$$Q' = (0.57/0.21)^2 Q \ , \tag{25a}$$

as suggested by (7) and (12). Here, Q is the dielectric value (Fig. 6) and (0.57/0.21) is the approximate ratio of the L[110] and $T_1[100]$ phonon frequencies. We also impose $\Upsilon = 14.1$, per Eq. (10a). This choice will be retained for all fits, since with $\Upsilon \gg 1$ the spectral profile becomes insensitive to Υ, as is easily seen from (13). With Q' given by (25a), the fits on 24 spectra have a mean chi square of 1.04, and the resulting bare frequencies are the open triangles in Fig. 13. They form a pronounced dip around 50 K, suggesting that the coupling $(Q')^{-1}$ given by (25a) is too small to account properly for the strength of the softening. The values of ν_c obtained in these fits are in reasonable agreement with the Vogel-Fulcher line of Fig. 10.

In a second attempt, ν_c is then fixed to the Vogel-Fulcher line, but Q' and ω_a are left free. These fits are systematically better, with a mean chi square of only 0.74. The results for $1/Q'$ are shown by the closed triangles in Fig. 14. Similar values of Q', only with more scatter, are also obtained in fits with five parameters free and solely Υ fixed. As seen from Fig. 14, the appropriate coupling is much higher than the dielectric prediction $(Q')^{-1}$. This is interpreted as an electrostrictive contribution following Eq. (23). In the region of the fits, the inverse coupling can be written

$$Q'' = 0.45 \times Q' \ , \tag{25b}$$

giving the short segment passing through the closed triangles in Fig. 14. Fitting now with Q'' fixed by (25b), the

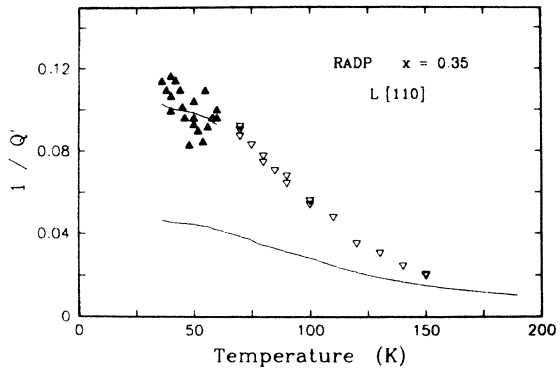

FIG. 14. Coupling parameter $1/Q'$. The lowest line is the value from the dielectric measurements (25a). The solid triangles are from fits with Q' and ω_a free. The upper line represents (25b). The open triangles are obtained using (18), as explained in the text.

results for ω_a and for ν_c shown by the closed triangles in Figs. 13 and 8, respectively, are obtained. The fits to the spectra are excellent. The values of ω_a are now much higher. They should be compared with the bare phonon frequencies (closed circles in Fig. 13) extracted from the coupled values at high temperatures ($T > 150$ K). They can be calculated using (25a) and (18), as the electrostrictive coupling is expected to vanish at high T where q^{EA} is zero.[13]

One sees that, contrary to the situation for the $T_1[100]$ mode (Fig. 8), the low-temperature bare frequencies do not fall on the Debye curve extrapolated from the high-temperature points (Fig. 13). We interpret this as an effect of the static polarizations $\delta \mathbf{P}^s$ [Eq. (19)]. Equation (21) only accounts for the dynamical changes $\Delta \mathbf{C}$ of the elastic stiffness tensor $\mathbf{C}$ owing to the coupling of the dynamical polarization fluctuations with the static ones. In addition, there are purely static changes associated with the development of the order parameter q^{EA}. These are, for example, the changes in the lattice constants which depart from the normal lattice anharmonic behavior.[30] In fact, the lattice parameter a shows an anomalous increase below ~ 100 K. Associated with this increase, one anticipates an anomalous decrease of the elastic constant C_{11}, and this is precisely what is observed in Fig. 13. To find a curve passing simultaneously through the high- and the low-temperature ω_a results, we assume that the anomalous decrease has the same shape as the birefringence anomaly, $3y^2 - 2y^3$, with $y = 1 - T/100$ for $T < 100$ K.[3]. Adding that function, with an adjustable prefactor, to the Debye curve of Eq. (8) with $\Theta = 384$ K, the best fit, illustrated by the solid line in Fig. 13, is obtained. The low-temperature extrapolation of the Debye function alone is illustrated by the dashed curve. One sees that the solid curve matches properly the 0-K extrapolation of the coupled frequencies (open circles). This should be the case, since dynamical couplings are expected to vanish at very low temperatures.

The cutoff frequencies obtained by leaving ω_a and ν_c free in the fits (closed triangles in Fig. 10) are systematically higher than those derived from the $T_1[100]$ spectra. The latter agree remarkably well with the Vogel-Fulcher line that interpolates data covering the range from ~ 100 to $\sim 10^{-4}$ cm^{-1}. We feel that this small deviation is not very significant as (i) fits with ν_c fixed to the Vogel-Fulcher line are practically equally good, and as (ii) the deviations might well be related to the approximations necessary in the treatment of the electrostrictive contribution. As we now have an estimate for the bare frequencies ω_a, one can calculate corresponding estimates of the coupling parameter $(Q')^{-1}$, using the coupled frequencies in the region 60 to 150 K and Eq. (18). The results are shown by the open triangles in Fig. 14, which interpolate smoothly between the low-temperature Q'' curve and the high-temperature Q' one.

Finally, the L[110] spectra give very clear evidence for the distribution of relaxation times and the associated dynamical CP. This is illustrated for one particular spectrum in Fig. 15. The solid curve is a good fit, as explained above. The spectrum shows clearly the following: (i) the phonon broadening, (ii) the dip at $\omega > \omega_B$, and (iii) the onset of a dynamical CP below ~ 0.2 cm^{-1}. Such spectra cannot be fitted without a distribution of relaxation frequencies. If instead of the rectangular distribution in (10b) we use a single Debye relaxation, we obtain the best fit shown by the dashed curve in Fig. 15. The latter fit has the same number of free parameters as the one shown with the solid curve, the distribution cutoff being simply replaced by the Debye frequency. The fit with the single Debye is unable to reproduce simultaneously the broadening of the phonon peak and the dynamical CP. In parameter space, one finds in this case two distinct minima, corresponding to either a good fit of the phonon width or to one of the CP. The inadequacy of the single Debye relaxation is most obvious between 30 and 40 K, as illustrated in Fig. 16, where the variances of the best fits obtained with a rectangular distribution of relaxations or with a single relaxation time are compared. Clearly, the distribution gives uniformly good results everywhere.

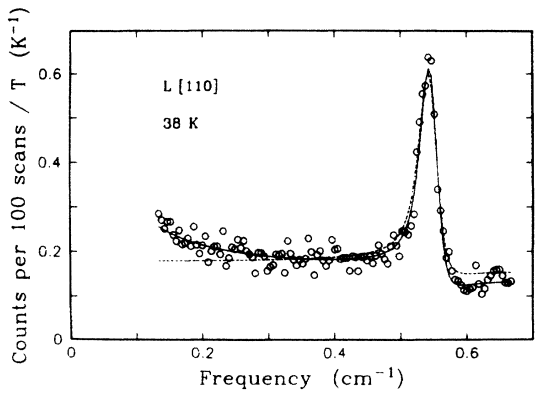

FIG. 15. L[110] spectrum illustrating the good fit obtained with a distribution of relaxations (solid line) and the bad one obtained with a single relaxation time (dashed line). The presence of a dynamical CP is very evident below ~ 0.2 cm^{-1}.

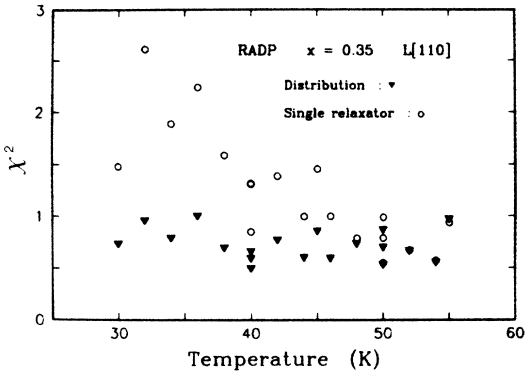

FIG. 16. Chi squares obtained from fitting with a distribution of relaxations and with a single relaxation time. The inadequacy of the single-relaxation fits is evident.

VI. DISCUSSION AND SUMMARY

The above analysis demonstrates that considerable information can be extracted from a line-shape study of Brillouin spectra on RADP glasses. It goes much beyond the mere observation of phonon softening. The central idea of the analysis is that the bare susceptibility, which can be characterized by a distribution of relaxation times owing to the collective effects in the glass, couples piezoelectrically and electrostrictively to the acoustic phonons. The spectra observed are due to the combined electro-optic and piezo-optic responses. By this approach, we have been able to obtain for the first time a complete description of the Brillouin line shapes associated with freezing phenomena in a structural glass. The experimental values obtained for the parameters of the theory are in excellent agreement with what has been found in other investigations, in particular dielectric-constant ones.

The two main results of this study are (i) the presence of a dynamical CP, and (ii) the adequacy of a broad distribution of relaxation times to describe the polarization response function. Brillouin scattering is not able to reveal much detail of that broad distribution. A distribution flat in $\ln\tau$ with a T-dependent long time cutoff was found to be fully consistent with the spectra. This cutoff is presented in Fig. 10. Although the Vogel-Fulcher law was used for that purpose, it must be emphasized that for the limited range of frequencies accessible to the Brillouin experiments, other laws could have been used just as successfully. It is only in combining experimental results covering a considerable frequency range that one might be able to compare somewhat meaningfully the different laws proposed for spin glasses.[7]

Unfortunately, the excellent quality of the crystals used in this study was still not quite sufficient to observe conclusively the central portion of the spectrum. The unresolved CP (whose frequency width is below the experimental resolution, see Fig. 11, and which will be called "elastic" in the following) was observed in all cases to grow upon cooling, and this particularly strongly below ~ 100 K. However, the size of this effect was not sufficiently reproducible to warrant a detailed report here. Thus, there seems to be room for two distinct CP's in the present system: (i) the "elastic" one, which might in fact be truly elastic and related to the "onset of freezing" as manifested in the natural birefringence,[3] the lattice parameters,[30] or also the static changes in the stiffness tensor illustrated in Fig. 13; (ii) a dynamic one, whose width is related to the low-frequency cutoff in the relaxation-distribution function, as discussed in the preceding sections.

We feel that Brillouin studies of the type presented here will become particularly important for investigations near the FE phase boundary in RADP. On the other hand, it is hoped that large crystals of superior quality can be produced that will allow conclusive results to be obtained on the "elastic" CP alluded to above. Finally, detailed line-shape analyses will be very valuable for other model glasses too, in particular, for the mixed alkali halide cyanides for which remarkable neutron results have been obtained,[31,32] but for which Brillouin studies have so far been restricted to reports of phonon softening.[33,34]

ACKNOWLEDGMENTS

Many thanks are expressed to Marcel Margot for his experimental assistance, in particular, for the automation of the data-acquisition systems and for the preparation of the oriented and polished single crystals. Laboratoire de Science des Matériaux Vitreux is Laboratoire No. 111 associé au Centre National de la Recherche Scientifiqu

*Present address: Laboratoire de Science des Matériaux Vitreux, Université de Montpellier II, F-34060 Montpellier, France.

†Present address: 23 avenue Général de Gaulle, F-72000 Le Mans, France.

[1]For reviews, see *Ill-Condensed Matter, Les Houches 1978*, edited by R. Balian, R. Maynard, and G. Toulouse (North-Holland, Amsterdam, 1979). For spin glasses, see K. H. Fischer, Phys. Status Solidi B **116**, 357 (1983); **130**, 13 (1985).

[2]Eric Courtens, Helv. Phys. Acta **56**, 705 (1983).

[3]Eric Courtens, J. Phys. (Paris) Lett. **43**, L-199 (1982).

[4]See, e.g., Sessions A8, A9, and P18, in *Proceedings of the Sixth International Meeting on Ferroelectricity, Kobe, Japan, 1985* [Jpn. J. Appl. Phys. **24**, Supp. 24-2, (1985)].

[5]E. Courtens and H. Vogt, J. Chim. Phys. **82**, 317 (1985).

[6]Eric Courtens, Jpn. J. Appl. Phys. **24**, Supp. 24-2, 70 (1985).

[7]Eric Courtens and Hans Vogt, Z. Phys. B **62**, 143 (1986).

[8]R. A. Cowley, Phys. Rev. B **13**, 4877 (1976).

[9]E. M. Brody and H. Z. Cummins, Phys. Rev. B **9**, 179 (1974).

[10]L. N. Durvasula and R. Gammon, Phys. Rev. Lett. **38**, 1081 (1977).

[11]E. Courtens, Phys. Rev. Lett. **41**, 1171 (1978).

[12]E. Courtens and R. Gammon, Phys. Rev. B **24**, 3890 (1981).

[13]Eric Courtens, Francois Huard, and René Vacher, Phys. Rev.

Lett. **55**, 722 (1985).
[14]L. Lundgren, P. Svedlindh, and O. Beckman, J. Magn. Magn. Mater. **25**, 33 (1981).
[15]Eric Courtens, Phys. Rev. Lett. **52**, 69 (1984).
[16]R. L. Reese, I. J. Fritz, and H. Z. Cummins, Phys. Rev. B **7**, 4165 (1973).
[17]C. Kittel, *Introduction to Solid State Physics,* 5th Ed. (Wiley, New York, 1976), p. 136.
[18]*Handbook of Mathematical Functions,* 7th printing, edited by M. Abramowitz and I. A. Stegun (Dover, New York, 1970), p. 998.
[19]H. Vogel, Z. Phys. **22**, 645 (1921); G. S. Fulcher, J. Am. Ceram. Soc. **8**, 339 (1925).
[20]Eric Courtens, Phys. Rev. B **33**, 2975 (1986).
[21]See, e.g., T. A. Litovitz and C. M. Davis, in *Physical Acoustics,* Vol. IIA, edited by W. P. Mason (Academic, New York, 1965), pp. 281—349.
[22]Eric Courtens, Phys. Rev. Lett. **47**, 868 (1981).
[23]R. Kubo, Rep. Prog. Phys. **29**, 255 (1966).
[24]K. Fossheim and J. O. Fossum, in *Multicritical Phenomena,* Vol. 106 of *NATO ASI Series B: Physics,* edited by R. Pynn and A. T. Skjeltorp (Plenum, New York, 1983), pp. 113—128.
[25]S. F. Edwards and P. W. Anderson, J. Phys. F **5**, 965 (1975).
[26]L. D. Landau and I. M. Khalatnikov, Dokl. Akad. Nauk SSSR **96**, 469 (1954).
[27]J. R. Sandercock, J. Phys. E **9**, 566 (1976).
[28]R. W. Gammon, E. Courtens, and W. B. Daniels, Phys. Rev. B **27**, 4359 (1983).
[29]D. W. Marquardt, J. Soc. Ind. Appl. Math. **2**, 413 (1963).
[30]Eric Courtens, T. F. Rosenbaum, S. E. Nagler, and P. M. Horn, Phys. Rev. B **29**, 515 (1984).
[31]J. M. Rowe, J. J. Rush, D. G. Hinks, and S. Susman, Phys. Rev. Lett. **43**, 1158 (1979).
[32]K. H. Michel and J. M. Rowe, Phys. Rev. B **22**, 1417 (1980).
[33]S. K. Satija and C. H. Wang, Solid State Commun. **28**, 617 (1978).
[34]C. W. Garland, J. Z. Kwiecien, and J. C. Damien, Phys. Rev. B **25**, 5818 (1982).